Chipping and wearing in MEMS inertial sensors: effects on stability and predictive analysis through test structures

Leonardo Gaffuri Pagani[1], Luca Guerinoni[2], Luca Falorni[2], Gabriele Gattere[2], Giovanni Mogavero[1,2], Aldo Ghisi[1] and Giacomo Langfelder[1]
Contact author email: leonardo.gaffuri@polimi.it
[1]Politecnico di Milano, Italy and [2]ST Microelectronics, Cornaredo (MI), Italy

***Abstract*— Impacts between fixed and moving parts in capacitive MEMS inertial sensors can generate debris and wear that undermine the device stability. This work investigates the effects of impacts and friction between rotors and stoppers through dedicated test structures. After modeling the scenario, considering the impact kinetic energy and the tensile/ compressive nominal strength of silicon, different stopper topologies and collision angles are studied. Results show how impact kinetic energies, up to 40 nJ (velocities in the 1-3 m/s range for typical inertial sensor masses), correlate with silicon rupture and provide first guidelines for robust sensors design.**

***Keywords* — MEMS, stability, reliability, chipping, wearing**

I. Introduction

Stability of MEMS inertial sensors is undoubtedly the most critical and debated parameter for next-generation applications (AR/VR, navigation, automotive). On *short-medium terms*, stability is influenced by temperature changes (substrate bending [1], electronics phase drifts [2], quality factor and mismatch drifts [3] …). On a *long-term* perspective, stability is influenced by aging (package hermeticity, getter saturation…). Both topics were widely debated and alternative solutions to conventional architectures were proposed [4, 5].

There are however *single-shock events* [6] that can lead to offset or scale-factor sudden variations: Fig. 1 reports examples of proof mass *chipping* (a) and of debris generation due to *wearing* (b). If the so-generated polysilicon particles are trapped in between capacitive sensing plates, they change the capacitor geometry inducing the mentioned instability. For typical sensing capacitances of conventional accelerometers or gyroscopes, chips of the dimensions shown in the figure can cause relative capacitive changes up to few 0.1%. In another scenario, such particles may affect leakage or couplings between electrical paths. As this jeopardizes all other efforts to improve stability, it is for sure a topic deserving attention, though its modeling is unavoidably complicated. Therefore, this work focuses on the study of chipping- and wearing-inducing phenomena and their modeling.

II. Methodology and Test Structures

A. Developed test structures

Two different types of structures have been developed to study the results of, respectively, impact and friction phenomena between a moveable proof mass and fixed parts. The adopted process is the 25-µm-thick, polysilicon ThELMA micromachining by ST Microelectronics, widely adopted for the fabrication of inertial sensors [7]. Packaging is done through glassfrit bonding, featuring a getter material that yields a final in-operation pressure around 1 mbar [8].

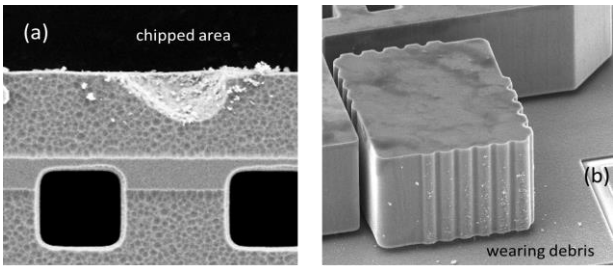

Fig. 1: scanning electron microscope (SEM) pictures of failures in inertial sensors due to (a) chipping of a portion of the suspended mass and (b) wearing effects on a stopper region (suspended mass removed for the sake of clarity). Size of the largest silicon chipped portion is as large as a µm³. Most of debris remain attached to the surface due to adhesion, but part of them moves away inside the package.

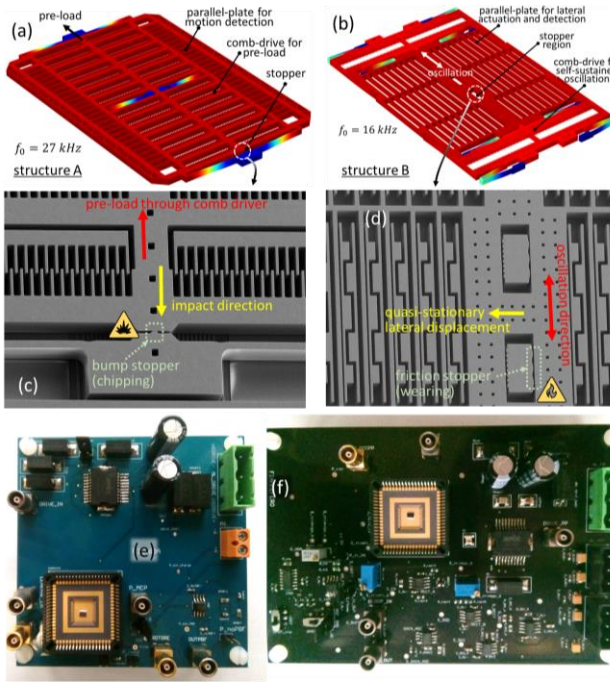

Fig. 2: structures developed to study the phenomena shown in Fig. 1. For chipping, a structure is pre-loaded by a large displacement and then released towards a stopper (a). For wearing, a structure is kept in oscillation and then laterally driven to soft friction on a stopper (b). SEM pictures refer to the contact area for impact (c) and for friction (d). The developed electronic printed circuit boards (PCB) including the MEMS test structures, wire bonded onto LCC68 carriers, are shown in (e) and (f).

This work was partly supported under the European Union ENIAC project ArrowHead Tools, grant agreement n. 826452.

- Structure-A is designed to provide strong in-plane impacts onto stoppers of different geometry: it embeds a large electrostatic comb actuator for pre-load and capacitive parallel plates for motion detection during and after impacts (Fig. 2a). In one variation, to add non-orthogonality to the impact, an additional plate is positioned underneath the mass, close to the impact area, so to generate an out-of-plane force component.
- Structure-B embeds an in-plane comb-driven resonator, kept in oscillation with a custom-designed electronic loop, and a lateral parallel-plate actuator that brings an oscillating wall to soft contact with a stopper, so to apply friction (Fig. 2b).

The resonance frequency of both structures (Tables I-II) is in the range of typical capacitive inertial sensors [9]. A scanning-electron microscope (SEM) zoom over the stopper region is provided for both the samples in Fig. 2c-d. Additionally, for each test device, variations of the bump shape (from almost flat to sharply edged) have been fabricated so to verify how this affects the shock or friction outcomes.

Table I: test structure-A parameters	
Resonance frequency	26100 Hz
Linear stiffness	285.97 N/m
Cubic stiffness	$5{\cdot}10^{11}$ N/m^3
Maximum preload	12.5 µm
Bump distance from proof mass rest position	0.8 µm
Proof mass	10.95 nkg
Quality factor	2600

Table I: electromechanical parameters of structure-A.

Table II: test structure-B parameters	
Drive resonance frequency	16500 Hz
Lateral resonance frequency	6623 Hz
Drive linear stiffness	179.53 N/m
Drive cubic stiffness	$2.456{\cdot}10^{11}$ N/m^3
Lateral mode stiffness	16.121 N/m
Oscillation preload []	12.5 µm
Friction bumper distance from rest position	0.8 µm
Drive mass	16.82 nkg
Lateral mode mass	9.31 nkg
Drive Quality factor	5640

Table II: electromechanical parameters of structure-B.

B. Impact kinetic energy modeling

A simplified impact model has been initially developed to predict the impact energy for structure-A as a function of the pre-load displacement, so to relate it to the nominal material strength. The proof mass is pre-loaded quasi-statically at the maximum available displacement (about 12.5 µm), accumulating a potential elastic energy (with a non-negligible mechanical nonlinearity) given by:

$$E_P = \frac{1}{2}kx_{PRE}^2 + \frac{1}{4}k_3x_{PRE}^4 \qquad (1)$$

where k and k_3 are the linear and cubic stiffness of the springs and x_{PRE} is the maximum preload. As the rotor is then abruptly released and the Q factor is very large, the energy is converted into its kinetic component (the loss during the first half harmonic cycle can be considered negligible).

Since the bumper is 0.8 µm away from rest position, some of the energy will be re-converted to potential. Substituting Eq. (1) in the well-known formula for the kinetic energy the following expression is obtained for velocity at the contact position x_{IMP}:

$$v_{IMP} = \sqrt{\frac{2\left[\frac{1}{2}k(x_{PRE}-x_{IMP})^2+\frac{1}{4}k_3(x_{PRE}-x_{IMP})^4\right]}{m}} \qquad (2)$$

Considering the designed test structure, the maximum kinetic energies that can be delivered to the stopper are in the order of 25 nJ. Such value is largely beyond the nominal rupture energy, whose 1st-order estimation can be derived by equating to the nominal strength (about 3 GPa) to the maximum pressure p_0 obtained after the collision between a flat surface and a cylindrical surface of radius R and height h (which is the 25-µm polysilicon thickness in this case):

$$p_0 = \left(\frac{\frac{F}{h}E}{\pi R}\right)^{\frac{1}{2}} \qquad (3)$$

In the equation above, E is the Young's modulus (corrected through the Poisson's ratio), and F is the applied force between surfaces inferred from the impulse-momentum theorem using a conservative estimation for the energy-loss time interval (less than 2 µs). Further details on the modeling approach for chipping can be found in [10]. Ongoing modeling of wearing will be detailed in future works.

III. Validation and Measurements

Finite-element method (FEM) and MATLAB/Simulink behavioral simulations were exploited, respectively, to design the device and to model the whole system. This is also needed for the definition of performance requirements of the electronic actuation/readout boards, and later to validate the measurements against the model.

Suitable electronic printed boards, shown in Fig. 2e-f, were developed for the wide range of required testing conditions. These include electrostatic actuation at voltages larger than 300 V (structure-A pre-load, or structure-B lateral displacement, see model predictions shown in Fig. 3) and slew rates larger than 60 V/µs, needed to avoid the slowing down of the structure-A proof mass, when sudden release occurs. Additionally, 2-MHz modulation test signals (1 V peak value) are required for motion monitoring with ~1 µs temporal resolution and sub-fF capacitive resolution.

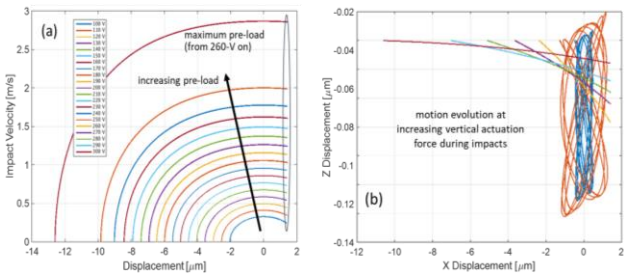

Fig. 3: model of structure-A impact velocity vs the pre-load voltage. Impact energies greater than 40 nJ are obtained for pre-load drive voltages >300 V. In case of simultaneous vertical actuation (b), consecutive impact angles with out-of-plane components are obtained (note the different scale between x and y axis in the figure).

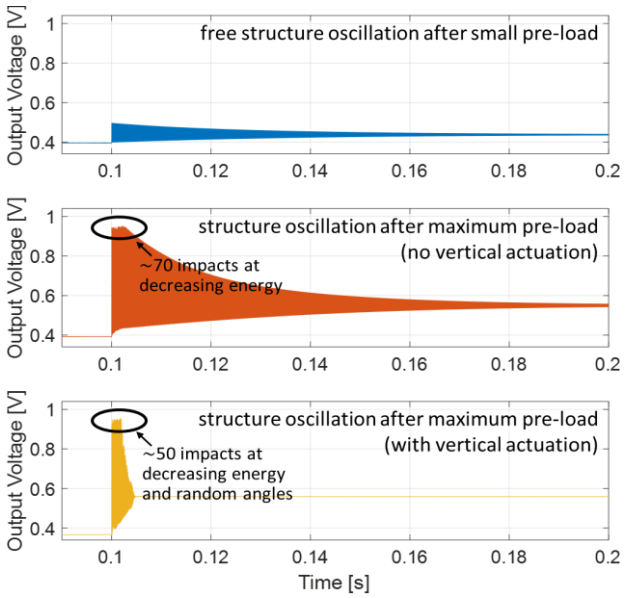

Fig. 4: response of structure A to small (top, no impact with the stopper) and large pre-loads. In the latter cases (center and bottom), consistently different energy loss is observed if impact is not just directed in-plane, orthogonal to the stopper, but has a vertical component (non-zero out-of-plane angle), which in the end causes a vertical pull-in that blocks the structure motion.

A. *Shock impact between proof mass and stoppers*

First tests are performed on structure-A: Fig. 4 reports experimental motion detection after release for a structure pre-loaded to displacements causing (i) no impact, (ii) in-plane impact and (iii) combined in-plane and out-of-plane impact. Motion evolution agrees with predictions, from which one empirically estimates the effective impact energy. Damage is never found for collision energies lower than ~2.5 nJ, corresponding to about 0.7 m/s impact velocity of the 10-nkg mass onto the stopper. On the contrary, damage is clearly found when the impact energy grows to 25 nJ, corresponding to 2.2 m/s impact velocity. Verification of the presence of damage is, at the moment, done after the tests through (i) a careful opening of the package, (ii) a focus-ion-beam (FIB) attack of the suspending springs, (iii) a removal of the mass, and (iv) a following SEM analysis. Images of this procedure are shown in Fig. 5 for a sample result. It is evident how the tip of the bump is flattened by the repeated impacts, with generation of multiple splinters of μm-size dimensions.

B. *Preliminary tests of wearing structures*

Fig. 6 reports the simulated self-sustained oscillation of structure B coupled to the developed oscillator, before and after lateral displacement onto the stopper. After friction begins, oscillations damp down, and can still be self-sustained only up to friction coefficients of 10^{-2} [11]. Otherwise, the circuit is not capable to sustain motion, and the oscillation will be damped with a timescale that depends on the applied pressure (and thus applied friction coefficient).

For comparison, the experimental results show (Fig. 7) that friction occurs with a coefficient that, as expected, depends on the lateral voltage (contact pressure) and is always larger than the aforementioned value. Oscillation is indeed, for any of the studied situations, damped down linearly in time (shown *equivalent Q factors* are thus approximated values). The wearing interval lasts about 15 ms for the softest contact,

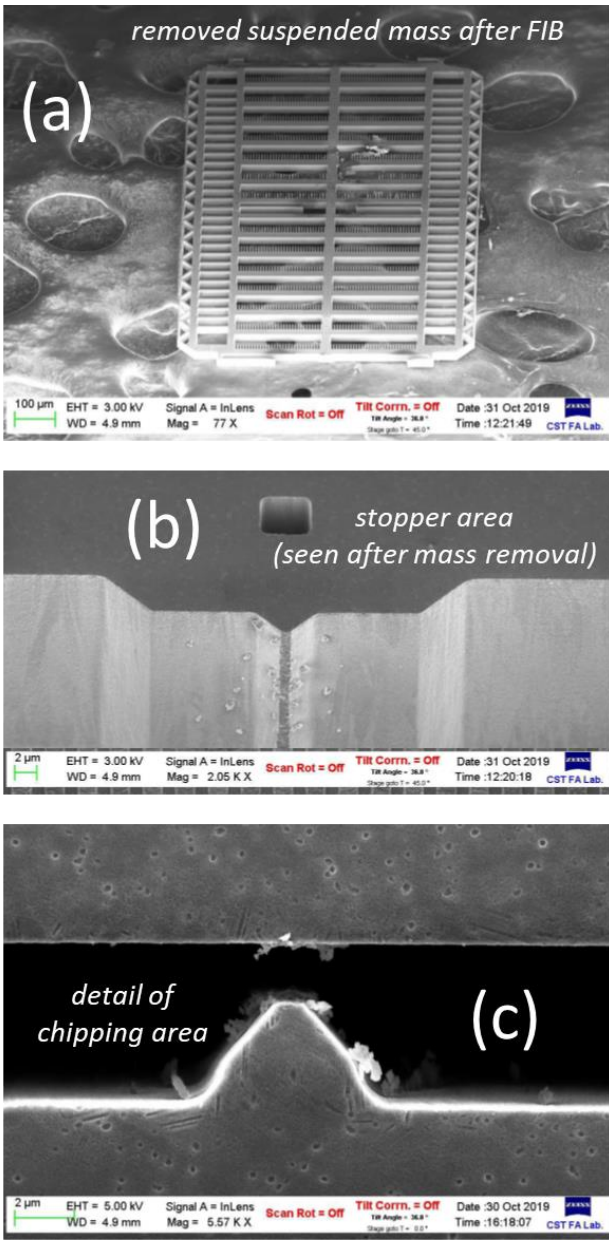

Fig. 5: SEM analysis of one tested Structure-A: the bird's eye views show (a) the rotor and (b) the stopper region after the FIB removal of the suspended mass. A closer detail of the same region is shown as a top view before the mass removal in (c): presence of chipped polysilicon particles is clearly visible.

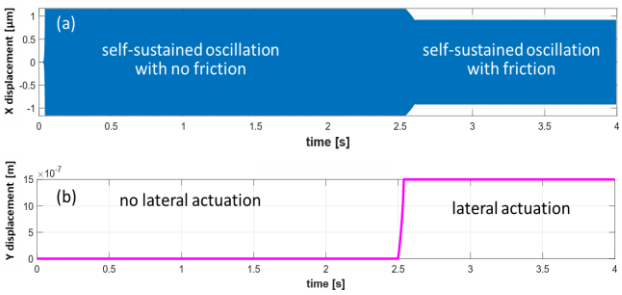

Fig. 6: self-sustained oscillation for structure B, before and after soft contact. The electronic design encompasses the possibility to hold the structure in oscillation even during wearing for friction coefficients lower than 10^{-2}. For larger friction coefficients (larger applied contact pressure) the oscillation will damp down after contact.

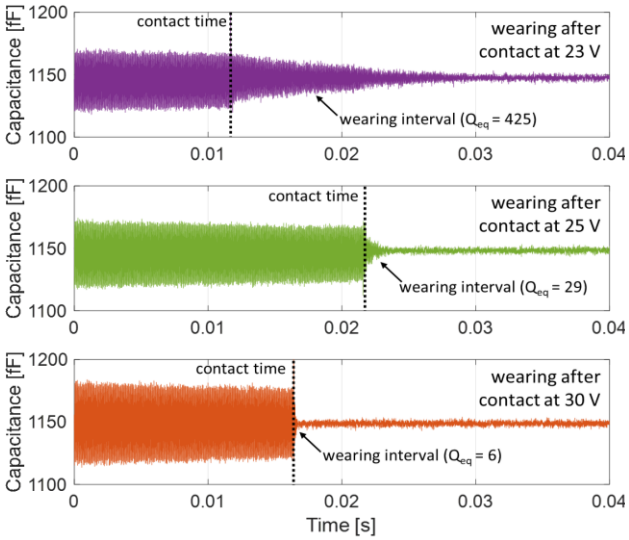

Fig. 7: measured damping of the oscillation due to friction as a function of the applied lateral voltage, which changes the pressure on the stopper and in turn friction. Note the equivalent Q changing vs applied pressure during friction.

and less than 1 ms for the strongest pressure onto the stopper. Package opening, FIB, and SEM analyses are ongoing for the tested structures to check for damage occurrence as a function of the friction pressure.

IV. Conclusions and Future Work

The work preliminarily introduced two types of test structures to study chipping and wearing phenomena in MEMS inertial sensors. The structures are capable of emulating various impacts and frictions scenarios that can occur throughout the lifetime of an inertial sensor. Repeatable generation of chipping effects is obtained for impact energies as large as 25 nJ, with no effects, instead, measured for impact energies lower by about an order of magnitude. For what concerns friction, the structure operation has been demonstrated but the analysis of friction effects is ongoing.

The multiplicity of testing parameters (impact energy, impact angle, bump geometry, bump distance, wearing pressure…), however, makes a larger statistical analysis necessary to draw safe design guidelines. This is made difficult by the challenges in identifying and quantifying the occurrence of damages without opening the structures (a long, and complicated process that does not lend well to statistical analysis on a large number of samples).

To this purpose, the structures have been redesigned by adding sort of *leakage paths*, formed by side-by-side interdigitated interconnections, positioned underneath the contact regions. It is expected that, after damage occurrence, chips or debris falling onto these paths may change the leakage resistance in between these buried interconnections. Correspondingly, a board redesign is also required to add this further measurement functionality.

References

[1] A. Tocchio, F. Rizzini, C. R. Marra, F. M. Ferrari and G. Langfelder, "Electro-mechanical chopping & modulation of acceleration: The geometry-modulated accelerometer," *2018 IEEE International Symposium on Inertial Sensors and Systems (INERTIAL)*, Moltrasio, 2018, pp. 1-4.

[2] S. Facchinetti, L. Guerinoni, L. G. Falorni, A. Donadel and C. Valzasina, "Development of a complete model to evaluate the Zero Rate Level drift over temperature in MEMS Coriolis Vibrating Gyroscopes," *2017 IEEE International Symposium on Inertial Sensors and Systems (INERTIAL)*, Kauai, HI, 2017, pp. 125-128.

[3] S. Dellea, P. Rey and G. Langfelder, "MEMS Gyroscopes Based on Piezoresistive NEMS Detection of Drive and Sense Motion," in *Journal of Microelectromechanical Systems*, vol. 26, no. 6, pp. 1389-1399, Dec. 2017.

[4] S. A. Zotov, B. R. Simon, G. Sharma, A. A. Trusov and A. M. Shkel, "Utilization of mechanical quadrature in silicon MEMS vibratory gyroscope to increase and expand the long term in-run bias stability," *2014 International Symposium on Inertial Sensors and Systems (ISISS)*, Laguna Beach, CA, 2014, pp. 1-4.

[5] M. H. Asadian, S. Askari and A. M. Shkel, "An Ultrahigh Vacuum Packaging Process Demonstrating Over 2 Million Q-Factor in MEMS Vibratory Gyroscopes," in *IEEE Sensors Letters*, vol. 1, no. 6, pp. 1-4, Dec. 2017, Art no. 6500104.

[6] S. Dellea, F. Giacci, P. Rey, A. Capodici and G. Langfelder, "Reliability of gyroscopes based on piezoresistive nano-gauges against shock and free-drop tests," *2016 IEEE 29th International Conference on Micro ElectroMechanical Systems (MEMS)*, Shanghai, 2016, pp. 255-258.

[7] G. Langfelder, C. Buffa, A. Frangi, A. Tocchio, E. Lasalandra and A. Longoni, "Z-Axis Magnetometers for MEMS Inertial Measurement Units Using an Industrial Process," in *IEEE Transactions on Industrial Electronics*, vol. 60, no. 9, pp. 3983-3990, Sept. 2013.

[8] B. Kim *et al.*, "Temperature Dependence of Quality Factor in MEMS Resonators," in *Journal of Microelectromechanical Systems*, vol. 17, no. 3, pp. 755-766, June 2008.

[9] J. Marek, "MEMS Technology- from Automotive to Consumer," *2007 IEEE 20th International Conference on Micro Electro Mechanical Systems (MEMS)*, Hyogo, 2007, pp. 59-60.

[10] M. J. Puttock e E. G. Thwaite, "Elastic Compression of Spheres and Cylinders at Point and Line Contact", *National Standards Laboratory Technical Paper N. 25*, Commonwealth Scientific and Industrial Research Organization, Australia, 1969.

[11] J.H. Horng, C.C. Wei, Y.Y. Chen, C.H. Huang, "Contact Friction Analysis of Silicon Material", *International MultiConference of Engineers and Computer Scientists 2009*, Hong Kong, pp. 1765-1768, ISBN:978-988-1701275, 2009.